

Experimental study of a pretensioned connection for modular buildings

Yujie Yu ^{*1}, Zhihua Chen ^{2a} and Aoyi Chen ^{3b}

¹ School of Civil Engineering, Central South University, No. 22 Shaoshan South Road, Changsha, Hunan 410075, China

² Department of Civil Engineering, Tianjin University, No. 92 Weijin Road, Nankai District, Tianjin 300072, China

³ Tianjin Architecture Design Institute, No. 95 Qixiangtai Road, Hexi District, Tianjin 300074, China

(Received April 17, 2018, Revised February 19, 2019, Accepted April 9, 2019)

Abstract. Modular steel buildings consist of prefabricated room-sized structural units that are manufactured offsite and installed onsite. The inter-module connections must fulfill the assembly construction requirements and soundly transfer the external loads. This work proposes an innovative assembled connection suitable for modular buildings with concrete-filled steel tube columns. The connection uses pretensioned strands and plugin bars to vertically connect the adjacent modular columns. The moment-transferring performance of this inter-module connection was studied through monotonic and cyclic loading tests. The results showed that because of the assembly construction, the connected sections were separated under lateral bending, and the prestressed inter-module connection performed as a weak semirigid connection. The moment strength at the early loading stage originated primarily from the contact bonding mechanism with the infilled concrete, and the postyield strength depended mainly on the tensioned strands. The connection displayed a self-centering-like behavior that the induced deformation was reversed during unloading. The energy dissipation originated primarily from frictional slipping of the plugin bars and steel strands. The moment transferring ability was closely related to the section dimension and the arrangements of the plugin bars and steel strands. A simplified strength calculation and evaluation method was also proposed, and the effectiveness was validated with the test data.

Keywords: modular steel building; inter-module connection; pretensioned strand; moment resistance; hysteresis performance

1. Introduction

Prefabrication using off-site manufacturing leads to faster construction, improved quality, and reduced resources and waste. Therefore, considering the rise in labor costs and environmentally friendly construction requirements, the advantages and the need for prefabricated structures have become increasingly obvious. A modular steel building is a highly prefabricated system. The entire structure or building is composed of prefabricated room-sized structural units that are manufactured offsite and installed onsite (Lawson *et al.* 2014, Chen *et al.* 2019). Historically, the main use of modular construction has been in portable or temporary buildings. Currently, prefabricated construction technology with volumetric units is already used in a wide range of building types, including schools, hospitals, offices, and any other buildings that require cellular and repetitive rooms (Sharafi *et al.* 2017). Early modular structures and units were primarily made using lightweight steel frames (generally made of light steel C-sections) and wood frames in which the loads are transferred through the sidewalls. Applications of this module type are found mostly in low-

rise or mid-rise buildings (Srisangeerthan *et al.* 2018). If applying the modular construction to high-rise buildings, more demand has arisen on a validated resisting mechanism for lateral forces such as wind loads or seismic excitations (Gunawardena *et al.* 2016a, b). To solve this problem, Lawson suggested the cooperation of a corner-supported modular structure with separated lateral force resisting systems, such as braced-structure and reinforced concrete or steel cores. The modular units are designed primarily for axial compression resistance, with the inside core charging the lateral force resistance and the global stability capacity (Lawson *et al.* 2012). Similar concepts were later adopted in some practical high-rise modular steel building projects such as Atlantic Yards B2 in Brooklyn, New York (Farnsworth 2014).

Another key issue associated with modular construction is the behavior of modular connections (Annan *et al.* 2009, Liu *et al.* 2015, Wang *et al.* 2016). Because the units are prefabricated offsite and assembled onsite, two types of connections are used. One type is the intra-module joint inside the module that is typically direct-welded in a factory. The other type is the inter-module connection between adjacent modules that often requires bolting, plugging, or welding methods for onsite assembly. For the corner-supported modules, a gap is generally needed between the floor and ceiling beams to facilitate the bolting or welding work and to allow the mechanical and electrical facilities to run along the building (Lee *et al.* 2015). In certain cases, the inter-module gaps are limited, and the

*Corresponding author, Professor,
E-mail: yujiecsu@csu.edu.cn

^a Ph.D., Professor, E-mail: zhchen@tju.edu.cn

^b Ph.D., Engineer, E-mail: chenaoyi@tadi.net.cn

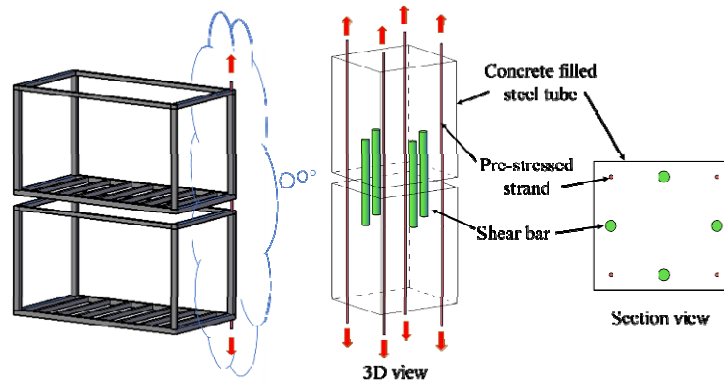


Fig. 1 Design and construction concept of the proposed inter-module connection

working space for connection assembly is insufficient. Then only the outer faces of the modular columns are accessible for connection during assembly (Fathieh and Mercan 2014, Annan *et al.* 2007). Several studies have investigated that how the unit connections and the inter-module connections could affect the capacity, robustness and seismic performance of the entire modular building. These studies demonstrated the significant importance of the connection performances in modular structure design (Fathieh and Mercan 2016, Doh *et al.* 2016, Lacey *et al.* 2018).

In recent years, the pretension technique has been gradually applied to prefabricated structures and assembled connections. Similar to posttensioned connections in self-centering steel frames, the tensioned connection uses posttensioned strands to connect steel beams to the column (Rojas *et al.* 2015, Lopezbarraza *et al.* 2016). Using the similar idea, a novel prestressed connection for the frame-type corner-supported modular steel buildings was proposed. The frame-type modular buildings generally contain no consolidated cores or bracing systems for lateral force resistance, and if they are used in high-rise buildings, the lateral loads or seismic effects produce tension force, shear, or moment loads between modules, which must be resisted or transferred through the inter-module connections. The proposed connection design uses the pretension technique for onsite assembly. The prestressed strands are used to resist the potential tension forces and to vertically connect adjacent modules to achieve integrality (Fig. 1). This design has comparatively clear force transmission mechanisms. Because no onsite welding is necessary, this design also meets the requirements for rapid assembly of multilevel or high-rise steel structures. An accompanying study for this new connection was performed in which a two-floor pretension assembled framed modular system was tested (Chen *et al.* 2017). The frame contained two modular units, and the vertically stacked modules were connected using the proposed pretensioned connection. The results indicated that the modular frame presented nearly elastic performance under fortified intensity shake earthquake levels. However, the detailed connecting performance of the connection and the working mechanism could not be obtained from the frame test study. In this study, a total of ten full-size model tests were conducted on the pretensioned vertical modular connections. First, six uniaxial loading tests were performed to explore the lateral

bearing performance, damage mechanisms, and rotational stiffness of the proposed connections. Second, four quasi-static cyclic loading tests were run to study the elastic and elastoplastic behaviors, energy dissipation capacity, and ductility performance. The test results can also aid in understanding the mechanical performance of similar pretensioned assembly connections.

2. Composition of the new pretensioned inter-module connection

The proposed inter-module connection for modular steel buildings uses prestressed strands to vertically connect modular columns and uses shear blocks across the assembled column sections to supply horizontal resistance to shear forces. The applied modular buildings are the corner-support type and use rectangular concrete-filled steel tubes as modular columns. The infill concrete is used to supply compression strength and support the encased tube to prevent local buckling. The high compression capacity of the concrete-filled steel tubes is especially suitable for column use in high-rise buildings. The detailed construction design and installation processes are illustrated in Fig. 2. The modular units are prefabricated using rectangular column tubes produced in a factory. Each column end has a stiffened seal plate with reserved holes for pass-through of prestressed strands and steel bars. The strand can be tensioned at each floor with use of the strand connectors between two connected column ends. Therefore, the pretension force in each column range can be controlled and modified. If one or several strands within a certain column range are damaged, the pretension force in the other floors does not suffer. A shear block is set at one column end, and the corresponding encasing hole is settled at the other end. The insertion of a shear block at the bottom column into the encasing hole at the upper column can supply the horizontal force resistance. The shear block is a small piece of hollow tube with a designed pouring hole to ensure concrete pouring. Plugin bars are installed across the assembled ends and anchored into the upper and bottom column to prevent concrete crushing and to strengthen ductility. Optionally, shear studs are added at the inside faces of the column tube to strengthen the bonding effect between the steel tube and the infilled concrete. The proposed inter-module connection

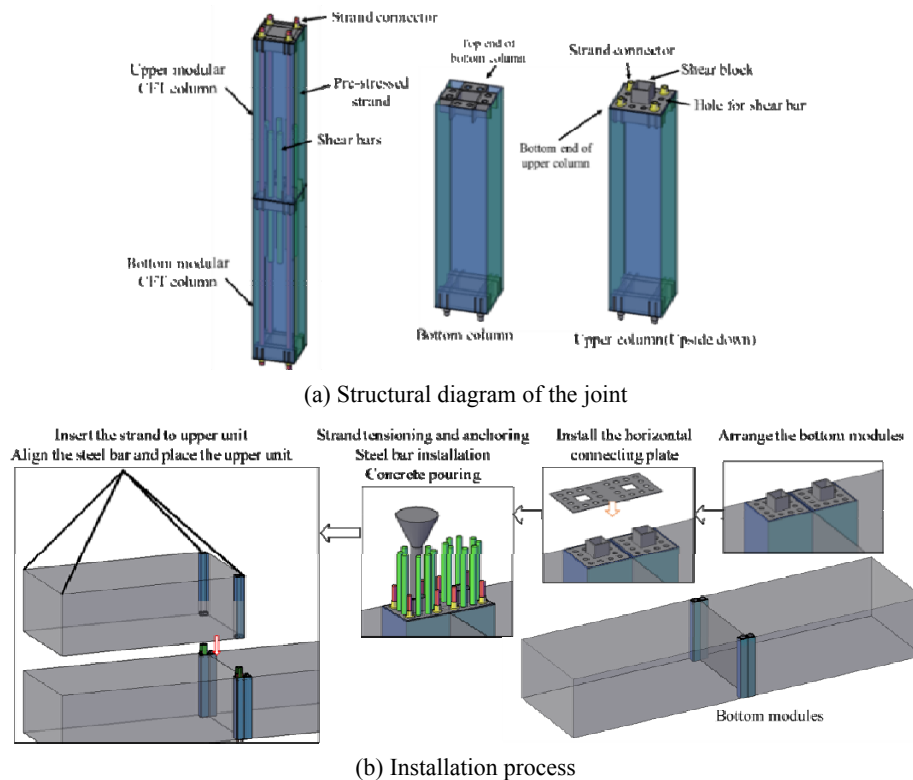


Fig. 2 Structural design and constructional erection of the proposed inter-module connection

is used to connect the vertical modules. The horizontal modules can be jointed together through a horizontal connecting plate, as shown in Fig. 2(b). The horizontal plate has drilled holes with a size similar to the peripheral dimension of the shear block, which can be used to horizontally fasten the adjacent shear blocks and the corresponding columns.

The primary modular assembly process is presented in Fig. 2(b). Once the bottom modules are placed at the desired location, the horizontal connecting plate is installed first. This plate has the same distributed holes as the seal plate, which forms a clamping mechanism with the shear blocks of the horizontally arranged columns. Second, the strands are stretched from the top side of the column, and the tensioned strands are locked with the strand anchors. The infill concrete is poured into the column tube through the shear block, and the steel bars are installed with the desired anchoring length. Because the steel tube itself can be viewed as the framework for concrete setting, there is no need for further templates for concrete pouring. The upper modules can be installed after the initial concrete curdle. When finishing the erection of the bottom floor modules, the upper floor unit is lifted above the desired location. The strands are inserted into the upper column with guiding lines, the steel bars and shear block are aligned to the reserved holes, and the upper unit is dropped into the designed place. Using the same connecting methods, the upper floor modules can be installed and fastened, and whole modular buildings can be finished in a floor-by-floor manner.

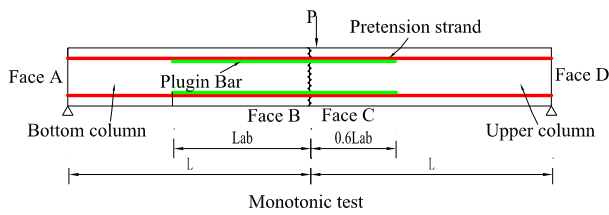
The modular building with the proposed inter-module connections has separate internal force-transferring paths.

The horizontal interaction between adjacent modules in the same floor is transferred through the horizontal plates, and the lateral shear and vertical loads between vertically stacked modules are transferred through the proposed pretensioned connection. Theoretically, this pretension design can ensure a highly tightened connection that can resist the potential moment, shear load, and unit separation trends in high-rise buildings under lateral loads. However, due to the particular construction of modular structures that have assembled unit joints and a separated load transferring mechanism, detailed studies are required.

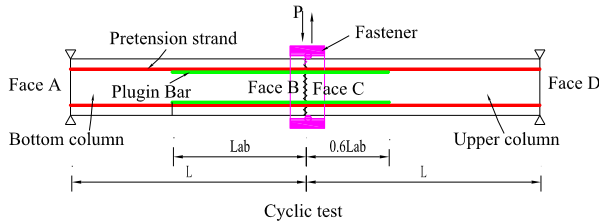
3. Test design

3.1 Loading plan

To investigate the stiffness and lateral force resistance of the prestressed inter-module connection, both monotonic loading and cyclic loading tests were performed. The tests were conducted at the structural lab of Tianjin University. The test specimen consisted of upper and bottom modular columns that were interrupted at the inflection point location, i.e., the mid-height of the columns. In this manner, the length of each column portion in the specimen was equal to half of the story height, and the boundary settings at the specimen ends could all be simplified as a pin joint (see the end constraints shown in Fig. 3). The monotonic and cyclic tests had the same loading phase in which the tested specimens were rotated by 90° and had simple supports at the two outer ends. The vertical displacement load was applied at one assembled column end in the



(a) Monotonic loading test



(b) Cyclic loading test



Fig. 3 Loading scheme and end constraint condition

middle of the specimen using a 1000 kN hydraulic jack. During monotonic static loading tests, the specimens were only subjected to downward compression. The two specimen ends were pin-supported at the bottom. During the quasi-static cyclic loading tests, a loading fastener was designed with a roller added at the upper and bottom ends to simulate the hinge support. The cyclic displacement load was realized using one fastener installed at the mid-span, and the pin-constraint boundary was ensured through additional fasteners installed at the two specimen ends (see Fig. 3).

3.2 Material properties

Steel type Q345B was used in all steel tubes and end plates, and all inside concrete consisted of grade C40 under the Chinese standard “Technical code for concrete filled steel tubular structures” (GB 50936-2014, 2014). The E43 electrode (with tensile strength greater than 430 MPa) was used in the complete penetration weld of the end plates. Each plugin bar used a 32 mm diameter HRB400 steel bar and had different anchorage lengths in the upper and bottom column. The plugin bar was anchored into the bottom column with a length L_{ab} of 1.0 m, which was calculated from the reinforced concrete design code (equation given in Appendix A). The plugin bar region that was anchored into the upper column had a welded anchor stud measure to increase the bonding with concrete. In this way, the required anchorage length can be reduced because a long anchorage length increases the difficulty for onsite alignment and insertion of the steel bars. Based on the design code of concrete structures (GB50010-2010 2010), the anchorage length with a welded stud can be reduced to 0.6 times L_{ab} , which was 0.6 m in the test. The length of the welded stud should be larger than 3 times the bar diameter. In the test, the other end of the plugin bar was welded with a 125 mm anchor stud at the end to strengthen the bonding effect, as shown in Fig. 3.

A total of two tube sections were considered: $360 \times 360 \times 10$ mm (width \times height \times thickness) and $250 \times 250 \times 10$

Table 1 Material properties of steel

Type	Characteristic strength	Yield strength	Ultimate strength
	f_d (MPa)	f_y (MPa)	f_u (MPa)
Steel tube-Q345B	295.0	395.1	542.7
Plugin bar-HRB400	360.0	412.0	638.9
Steel strand-Grade 1860	1860.0	1908.4	-

mm. Shear studs (when present) were settled with an interval of 100 mm at the inner column faces within a 800 mm range from the connected ends (800 mm from face B of the bottom column and from face C of the upper column). The pretension strand was 1860 grade with a diameter of 21.6 mm, and the yield strength of the steel strand was 1860 MPa. During specimen manufacturing, the plugin bars and strands were arranged and stretched prior to concrete pouring.

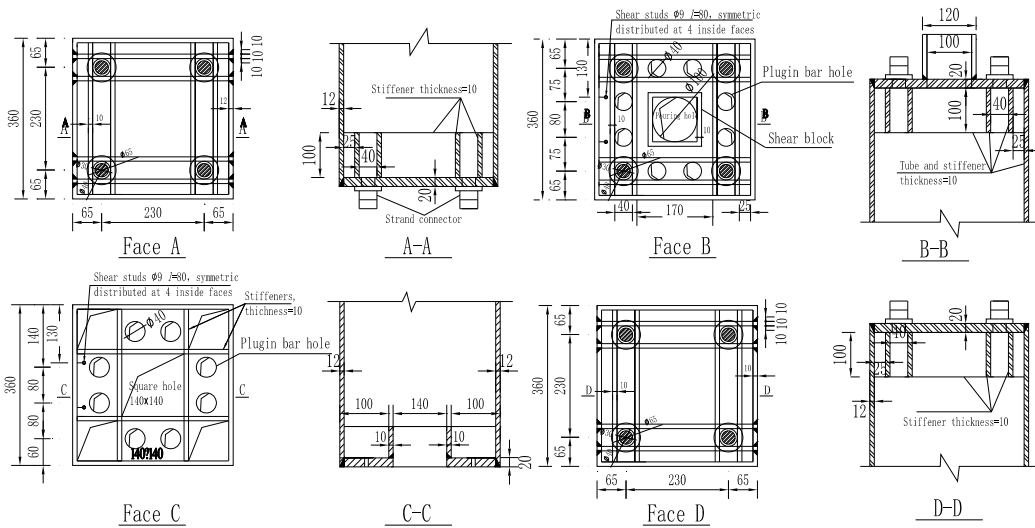
Connection details such as pretension force determination and the anchorage length calculations were all performed based on the characteristic material strengths in structural design. Before the connection experiments, standard material tests were conducted to obtain the real material strengths and verify the manufacturing qualities. Three coupons were tested for each steel grade, and the average measured steel material strengths are listed in Table 1. The 28d compressive and tensile strengths of the concrete were determined from standard cylinder compression and axial tension tests. The characteristic compression and tension strengths were 19.1 and 1.7 MPa, respectively (GB 50010-2010 2010), and the measured concrete strengths were 41.2 MPa in compression (f_c) and 3.3 MPa in tension (f_t).

3.3 Specimen design

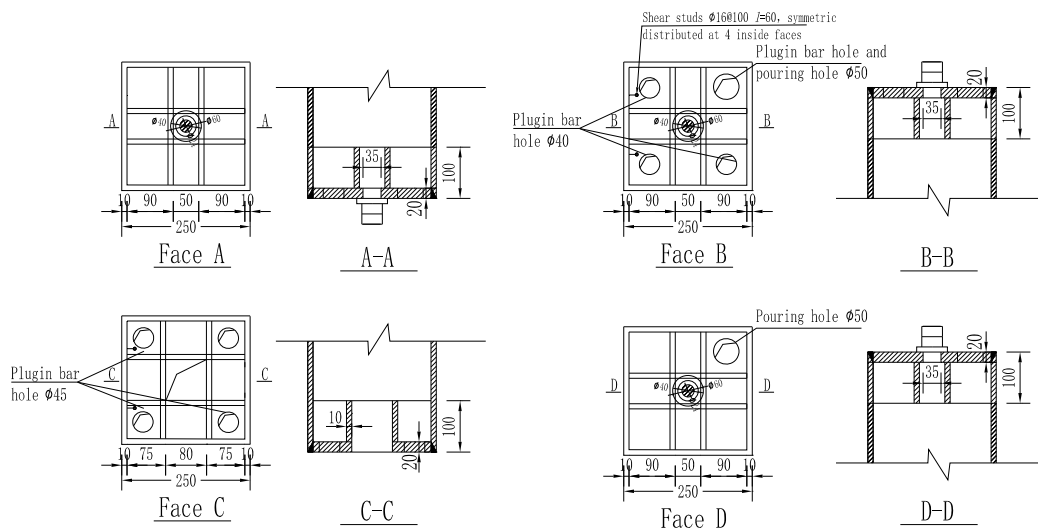
The experimental tests were designed to study the moment-bearing strength and stiffness characteristics and the influence patterns of different construction details such as column section, column length, shear studs, plugin bar, and pretension force. A total of six monotonic loading specimens (labeled S1-S6) and four cyclic loading specimens (labeled QS1-QS4) were designed. The detailed connection designs and dimensions of the tested specimens are given in Fig. 4, and the number and the studied factors of each specimen are summarized in Table 2.

Specimen S1 had the same column section configuration and pretension status as S2 but had no shear studs and plugin bars. The resulting differences between S1 and S2 can aid in understanding the contribution of the bonding effect. A comparison between S3 and S4, together with a comparison between S5 and S6, can be used to explore the effect of shear studs under both pretensioned and un-

tensioned conditions. Specimen S3 adopted a 6 m stretching method. In this case, the steel strands were stretched directly from the two specimen ends without the intermediate strand connector at the assembled sections. In contrast, specimen S4 used the separate stretching method (3 m stretching) in which the upper and bottom columns were separately stretched using intermediate connectors at the assembled ends. The comparison can indirectly reflect the pretension continuity effect on the lateral load resistance behaviors. S5 and S6 had no pretension strands, and the comparison between S1 and S5, together with the difference between S2 and S6, can be used to study the contribution of the pretension force and plugin bars. In the cyclic loading test, only wide-column section specimens were studied. QS1 and QS2 were used to investigate the column length effect, and difference between QS1 and QS3 can reflect the influence of pretension force distribution. QS1 and QS4 together can illustrate the shear stud contribution to the hysteresis performance.



(a) Construction and section details of S1-S2 and QS1-QS4



(b) Construction and section details of S3-S6

Fig. 4 Configuration details of specimens

Table 2 Number and dimension of the specimens

Type	Column section (mm)	Column length L (m)	Shear studs	Plugin bar	Prestressed strand	Pretension force
S1	360×360×12	1.5	No	No	Yes	0.4 fptk*
S2	360×360×12	1.5	Yes	Yes	Yes	0.4 fptk
S3	250×250×12	3	No	Yes	Yes	0.4 fptk (6 m stretch)
S4	250×250×12	3	Yes	Yes	Yes	0.4 fptk (3 m stretch)
S5	250×250×12	3	No	Yes	No	-
S6	250×250×12	3	Yes	Yes	No	-
QS1	360×360×12	3	Yes	Yes	Yes	0.4 fptk
QS2	360×360×12	1.5	Yes	Yes	Yes	0.4 fptk
QS3	360×360×12	3	No	Yes	Yes	0.4 fptk for bottom, 0.2 fptk for upper
QS4	360×360×12	3	No	Yes	Yes	0.4 fptk

1, fptk is the designed tension level of steel strand, which was 530 kN in the test

2, The pretension force “0.4 fptk” in the table without additional marks represents the direct stretching at two specimen ends

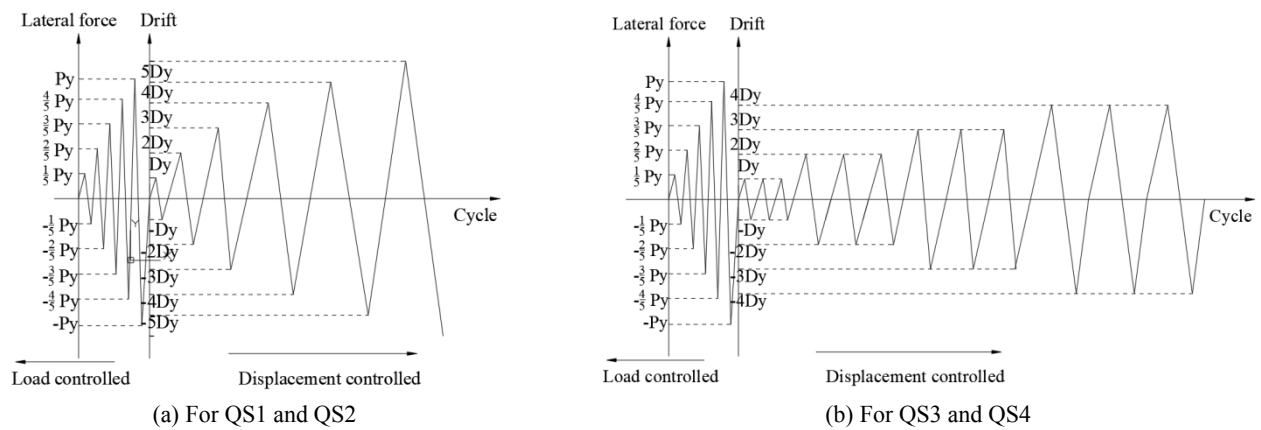


Fig. 5 Loading history

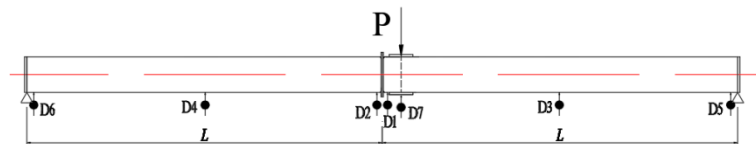


Fig. 6 Measurement plan

3.4 Loading scheme

The loading history for the quasi-static cyclic tests was generally based on the testing protocol specified in the Chinese Specification of Testing Methods for Earthquake Resistant Buildings (JGJ101-96 1996). The yield load P_y was predicted from the results of monotonic loading tests. Before the specimen yielded, the lateral force was controlled by load. In the load-controlled stage, lateral force was applied at five levels corresponding to $1/5$, $2/5$, $3/5$, $4/5$, and 1 times the predicted specimen yield strength. When connection yielding was observed (the tangent stiffness of the obtained load-displacement curve presented an obvious reduction), the lateral loading method was

changed to a displacement-controlled method with the lateral displacement increment as the monitored yield displacement D_y . Two displacement-controlled loading procedures were applied. For QS1 and QS2, the displacement steps adopted the increasing loading method in which the applied displacement increased with an amplitude of D_y and only one cycle at each displacement level (Fig. 5(a)). For the remaining specimens, each displacement amplitude was repeated for three cycles (Fig. 5(b)). The test was terminated when the vertically applied load could not be maintained, when the deflection deformation surpassed $1/50$ of the length of the column, or when the lateral force decreased below 85% of the maximum load.

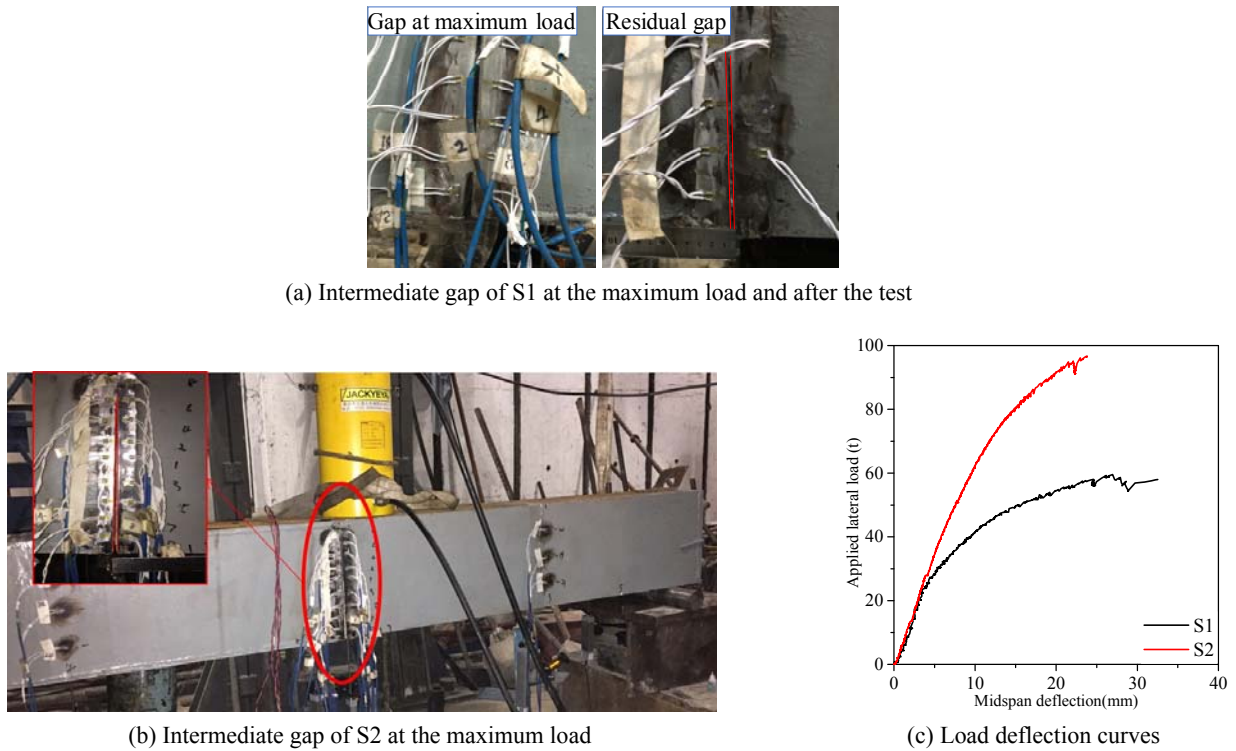


Fig. 7 Test results for S1 and S2 (monotonic tests on a wide 360 mm column section)

3.5 Measurement scheme

Because of the assembly construction, the connection specimen was opened up at the intermediate assembled sections. During testing, the vertical deflection, applied load, and strain were measured and recorded. The vertical loads applied to the specimen were automatically recorded by a loading cell in the hydraulic actuators. Seven displacement transducers (DTs) were mounted on the underside of the specimens to measure the specimen deflection, as shown in Fig. 6. A total of four DTs were located at both ends of each modular column (two DTs at the middle of the columns and one at the mid-span loading block).

4. Test results and analysis

4.1 Monotonic test behavior

Specimen S1 exhibited a linear load-deflection relationship in the initial stage. Under 4 mm of applied displacement, the load-deflection curve showed a decrease in tangent stiffness, representing slippage between the steel strands and the concrete. Because no shear studs and plugin bars existed for additional bonding (except for the tensioned strands), the assembled ends between the upper and bottom columns were separated early. As the vertical displacement load continued, the intermediate gap was increased. When the applied displacement reached 27.0 mm, the bottom steel strands experienced micro-adjustments, with sudden slippage and a certain decrease displayed at the lateral strength. At this point, the maximum separation gap

between the assembled sections reached 10 mm. The test stopped when the mid-span deflection reached 32.5 mm (surpassing 1/50 of the 1.5 m column length, i.e., 30 mm). When the specimen was unloaded, the intermediate gap was recovered and closed. However, a 3 mm residual gap remained between the assembled sections at the completion of unloading.

S2 had a strong bonding effect with the shear studs, plugin bars, and steel strands used in connection, and thus, it had strong lateral stiffness and load bearing ability. Under the same deflection, S2 had apparently higher strength than S1. Before the applied load reached 800.0 kN, the applied load versus displacement curve continued to increase linearly. Because of the limitation of the loading jack (0-1000 kN range), the test stopped at a lateral load of 967.0 kN, with a midspan deflection of 24.0 mm. An intermediate gap can also be observed between the assembled faces. However, the separation extent was smaller than that of S1, which was 6 mm under the maximum load (see Fig. 7(b)). The lateral strength of S2 still presented an increasing trend prior to test termination. Additionally, S2 had almost twice the lateral strength of S1, indicating the important contribution of shear studs and plugin bars to the connection performance (Fig. 7(c)).

Specimen S3 to S6 differed from S1 and S2 in the use of small-section construction and a long column length. These four specimens also exhibited negligible column bending but had an obvious intermediate gap between the assembled faces under lateral loading. However, the extent of this separation gap was much larger than those of S1 and S2. Specimen S3 showed a stable strength increase before the lateral displacement increased to 10.2 mm (corresponding to a 34 kN applied load). Slight concrete cracking sounds

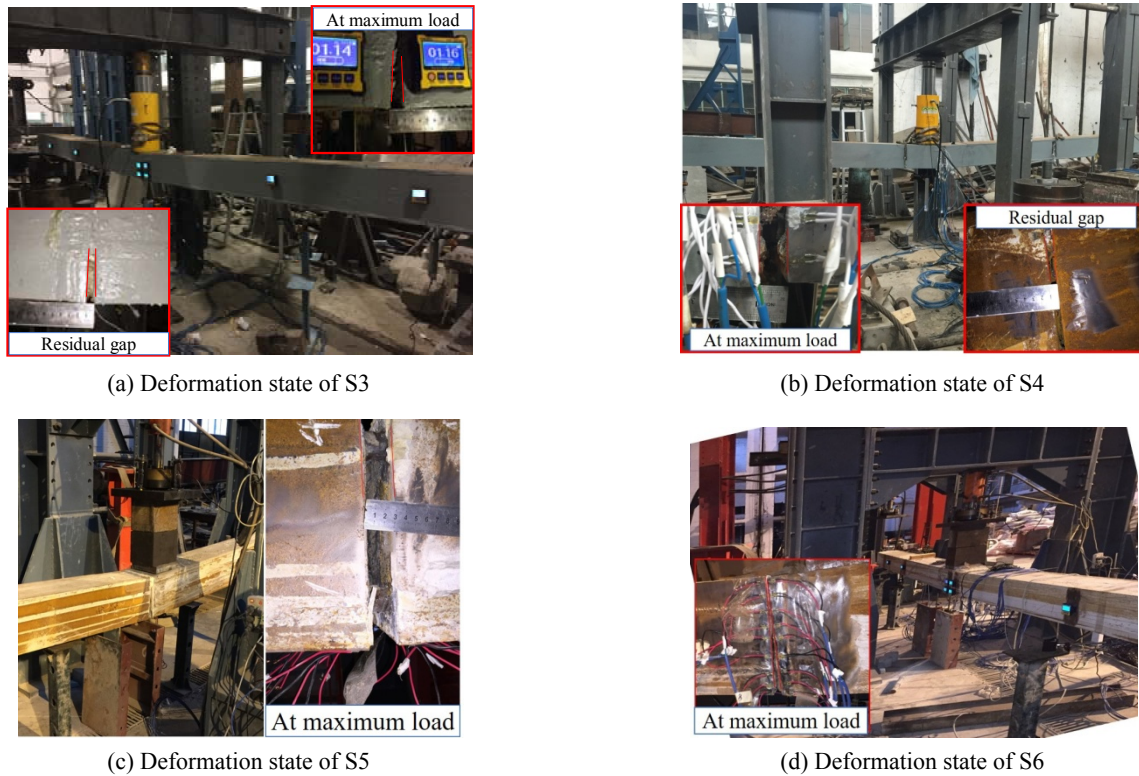


Fig. 8 Deflection and gap behavior of S4-S6 (with a small column section of 250 mm)

were produced, representing micro-slippage between the steel strands and concrete. Simultaneously, the assembled ends were separated, with decreased tangent stiffness at the load-deflection curve. The intermediate gap increased rapidly with increasing loading amplitude. When the midspan deflection reached 58.3 mm, the intermediate gap reached 20 mm, and the test was stopped. The bent specimen was recovered during the unloading process, with a residual gap of 8.0 mm at the completion of unloading. Specimen S4 had a deformation behavior similar to that of S3 but with larger lateral bending strength and better ductility. When the applied deflection reached 44.3 mm, the lateral strength stopped increasing and remained constant at 94.0 kN. The maximum intermediate gap was 25.0 mm with a midspan deflection of 71.2 mm, and the separation gap returned to 5.0 mm after unloading.

Specimen S5 and S6 contained plugin bars but no pretension strands, and S6 had shear studs inside the steel tube. Without the pretensioned strands to hold the two columns, the lateral bending resistance of the connection was dramatically reduced. Specimen S5 exhibited some strength drops during lateral loading, and accompanying these strength drops, concrete crushing and falling behaviors occurred, which indicated slippage between the plugin bars and concrete. Specimen S5 reached its maximum strength with a midspan deflection of 27.2 mm. The lateral strength decreased rapidly, and the intermediate gap was 10.0 mm at the maximum strength state. The reason for this low ductility and rapid strength deterioration was the weak bonding mechanism between the assembled column. The bonding mechanism between the plugin bars and concrete was the only axial force transmission path

between the upper and lower modular columns, and this bonding relation was fragile such that once the bonding failed, the subsequent deterioration was rapid. Specimen S6 had strength and ductility performance similar to that of S5, indicating that the shear studs did not present much effect on the axial force transmission for the proposed connection.

Fig. 9 shows the obtained load deflection curves of S3 to S6. The four specimens all presented a similar initial stiffness. During this period, the connection remained in the completely bonded state in that no slippage occurred, and the lateral strength was mainly attributed to the section dimensions. Specimen S4 to S6 showed a steady strength increase between 10.0 and 20.0 mm midspan deflection, whereas the stiffness of S3 began to decrease due to strand slips. This difference indicated that the plugin bars participated in the load transfer at the early loading stage through contact bonding to concrete. If plugin bars were presented for axial connection, the moment strength of the connection was expected to decrease rapidly after the initiation of slipping, as in specimen S5 and S6. For specimen S4, the concrete bonding to the plugin bars and strands cooperated at first, but when the midspan deflection reached 25 mm, the concrete bonding with plugin bars was gradually lost and left only the tensioning and contact bonding at the steel strands for axial connection. As the vertical deflection continued, the strand bonding also stopped working, the tension force at steel strands remained, and the moment strength of the connection stopped increasing. The shear studs had a slight strengthening effect on holding the concrete, but the influence on the contact bonding mechanism and the connection moment strength was weak.

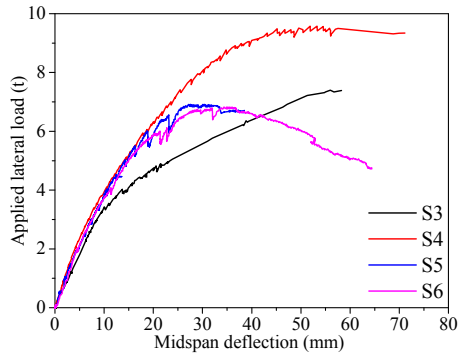


Fig. 9 Load deflection curves for S4-S6

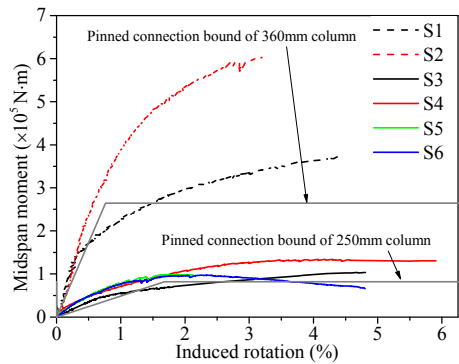


Fig. 10 Moment rotation curves of static tests

The concrete-filled steel tube column remained straight during the entire loading process, and the vertical deflection of the assembled specimen originated mainly from separation of the assembled ends. Fig. 10 shows the midspan moment-rotation relations of the six specimens. The connection rotation was calculated as the sum of rotation changes between the upper and bottom modular columns (as explained in Appendix B). A generally used connection rigidity classification guide is the European Code 3 Part 1-8 (EN 1993-1-8 2005), which states that the rigidity of the frame connection can be classified as rigid, semirigid and pin connection with bounding lines of 25 times and 0.5 times the linear stiffness of the connected members for sway frames. From the point of moment strength, the connection can be classified as a full-strength, partial-strength and nominally pinned connection with boundaries of 0.25 times and 1.0 times the design plastic

moment resistance of the connected beams. The inter-module connections of the modular steel buildings were commonly simplified as pin joints in structural design, but the correctness of this simplification still lacked verification. Currently, no design guidance and classifications are available for inter-module connections, and previous design processes for the modular buildings still all referred to the design methods for steel frame structures. Referring to the joint classification methods in EC3, the lower bound between the semirigid and pinned connections was calculated from the linear stiffness and plastic moment resistance of the connected columns, as shown in the plot of Fig. 10. These prestressed inter-module connections had an initial stiffness and connection strength that were slightly larger than but quite close to the lower bound. Therefore, this connection can be treated as a pin joint for safety consideration, even with the pretension used in the connections.

4.2 Cyclic loading tests

Similar to the behaviors in the monotonic test, the connected modular columns remained straight throughout the loading process, and the vertical displacement load primarily led to the separation gap between the assembled faces. For QS1, the load-deflection relation was linear during the initial loading stage. When the applied load reached 434.2 kN, the connection exhibited a stiffness change, with a Δy value of 67.9 mm. The loading protocol changed to a displacement-controlled process. In the subsequent loading process, the concrete crushing and strand slipping sounds continued to occur. When the midspan deflection reached $2\Delta y$, the intermediate gap reached 15 mm, and the lateral strength started to show degradation. During the subsequent $3\Delta y$ loading stage, concrete crushing became intense, and small concrete pieces scattered down from the opening. The separation gap increased to 28.0 mm with the $3\Delta y$ midspan deflection. During reverse loading of the first $3\Delta y$ cycle, the lateral strength was further degraded and quickly dropped below 85% of the maximum strength. At this point, the test was stopped.

For specimen QS2, the assembled faces started to present separation under 60.0 kN of applied load, and concrete crushing sounds occurred under when the applied load reached 350.0 kN. The connection yielded at 880.7 kN, with a 10 mm (Δy) midspan deflection. Displacement-



(a) Deflection pattern at Δy load



(b) Deformation at $2\Delta y$



(c) Intermediate gap

Fig. 11 Test results of QS1

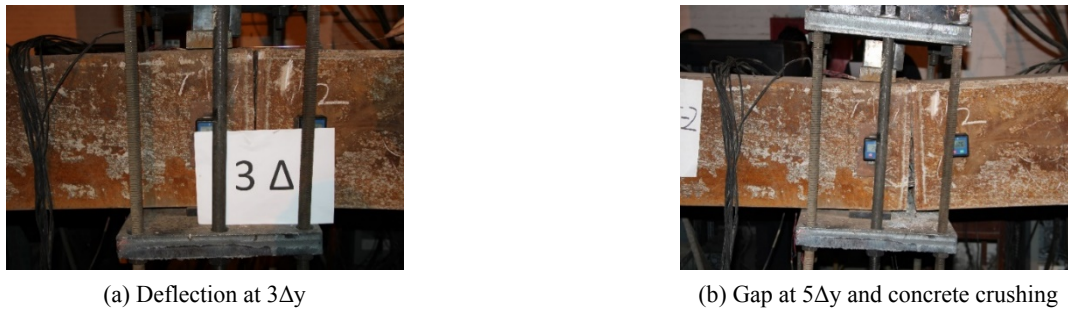


Fig. 12 Test results of QS2



Fig. 13 Test results of QS3

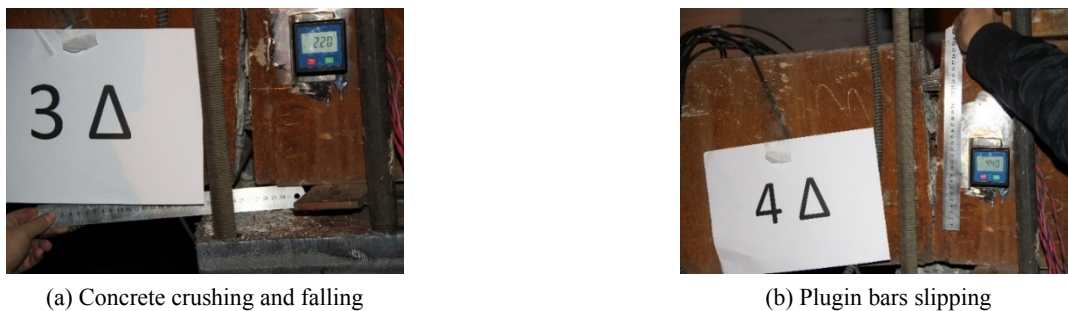


Fig. 14 Test results of QS4

controlled loading was used. During the subsequent loading process, the moment-bearing strength gradually increased, and the elastic modulus decreased. The connection reached its maximum lateral bearing strength during the $3\Delta y$ loading cycle, which occurred at 998.6 kN with an intermediate gap of 10.0 mm. The concrete crushing and plugin bar slippage became more severe, and the steel strands were obviously bent by the surrounded concrete. Moreover, the upper and lower modular columns were dislocated. The steel strands exhibited wire breakage during $5\Delta y$ loading with loud sounds, at which moment the intermediate gap reached 20.0 mm. As concrete crushing continued to spread within the connected region, and the lateral strength continued to decrease. During the $6\Delta y$ loading, the intermediate gap reached 30.0 mm, and the lateral strength was reduced to 790.9 kN (79% of maximum loading). At this point, the test was stopped.

Specimen QS3 exhibited yield behavior at a midspan deflection (Δy) of approximately 40 mm with a 485.1 kN applied load. At this point, a 25 mm separation gap already had appeared between the assembled faces. During the

subsequent loading process, the plugin bars and strands gradually displayed slipping behaviors with the increase in applied displacement. The concrete bonding to the plugin bars and the steel strands supported the lateral strength increase during the first cycle; however, this bonding mechanism was gradually lost, and the slippage range was increased during the subsequent loading process. The first cycle of each deflection level ($2\Delta y$ and $3\Delta y$ deflection load levels) generally presented a certain strength increase, but the elastic stiffness and strength were gradually decreased during the subsequent 2nd and 3rd cycles. The lateral bearing strength of the connection peaked during the first $2\Delta y$ cycle. During the first $4\Delta y$ loading, the strand was damaged under severe bending, together with a loud sound and a sudden drop in the lateral strength. The intermediate gap reached 50 mm, and crushed concrete emerged from the separated ends. During the subsequent reverse loading, the lateral strength dropped to 281.9 kN, which was approximately 60% of the maximum load. At this point, the test was stopped.

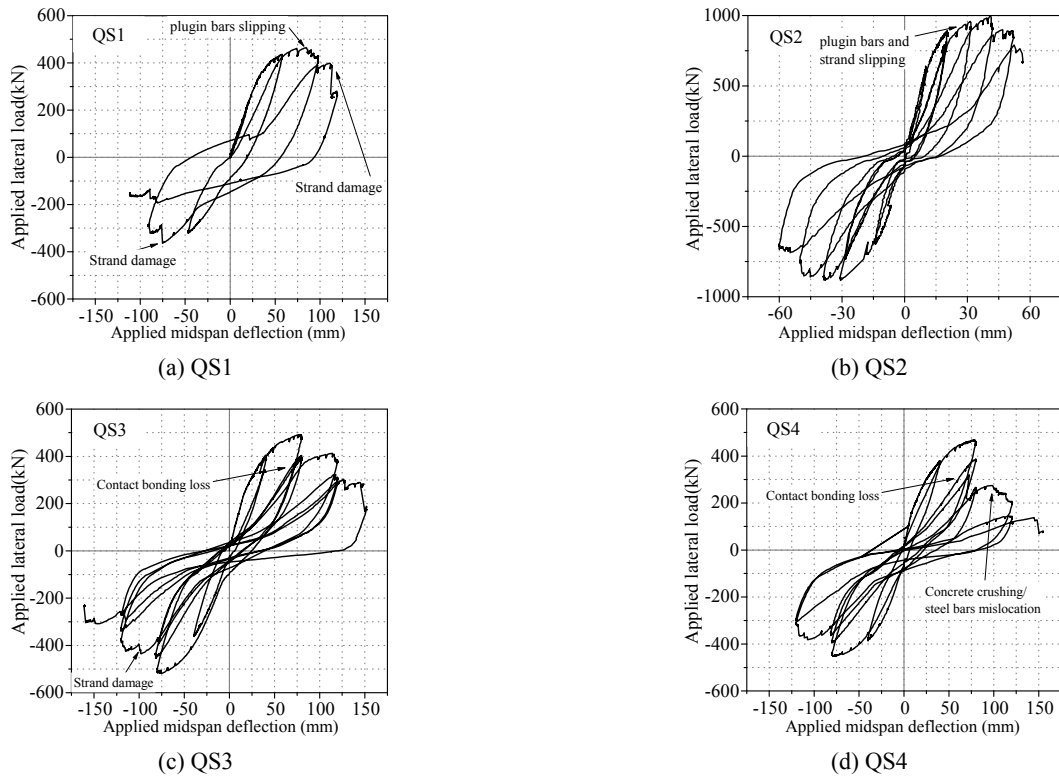


Fig. 15 Applied load deflection curve in cyclic tests

Specimen QS4 had a yield strength of 464.9 kN, with a midspan deflection Δy of 40 mm. QS4 reached its peak lateral strength of 464.2 kN during the first $2\Delta y$ cycle, followed by apparent strength and stiffness degradation due to concrete crushing and slipping. The lateral strength dropped to 273.9 kN during loading of the first $3\Delta y$ cycle. Concrete pieces fell from the gap, and plugin bar slipping sounds occurred. Due to the obvious strength degradation, the dramatic gap, and obvious slipping behaviors, the test was terminated after the last cycle of $3\Delta y$ loading.

Fig. 15 shows the obtained applied load versus displacement relations during cyclic tests. The hysteresis loops all displayed obvious pinching phenomena, characterized by a self-centering double-flag shape similar to the hysteresis curves of typical steel-reinforced concrete connections. Because of the unintegrated columns and the assembled connection construction, the assembled sections became separated under lateral loads, but the gap closed during unloading due to the presence of the tensioned strands; further, the lateral strength of the specimens returned to the origin point with little residual deflection. The double flag region in the hysteresis loops was mainly attributed to frictional sliding between the concrete and the plugin bars or steel strands. Specimen QS1 and QS2 adopted the increased amplitude loading protocol without repeat cycles. This loading method led to greater load-transferring participation at the bonded region before considerable slippage occurred. The lateral strength displayed a continued strength increase, especially in QS2. The strength degradation in latter cycles of QS1 mainly resulted from failure of concrete bonding and the resulting slipping behaviors. For specimen QS3 and QS4, three

cycles were adopted at each deflection level. The lateral load-bearing performance in the two repeated cycles degraded dramatically, and the residual strengths at the two cycles mainly originated from the holding effect of pretensioned strands and frictional sliding at the surface of the steel strands.

5. Discussion of results and simplified calculations

5.1 Cyclic test data discussion

The hysteresis results in Fig. 15 only displayed the applied load conditions. However, because different modular column lengths were adopted, the lateral load comparison cannot truly reflect the moment-transferring ability at the assembled connection. The relations between the midspan moment and the induced connection rotation were obtained and compared (Fig. 16). Due to the same section dimension of the four tested specimens and similar plugin bar and strand settings, the resulting moments at the assembled sections were quite similar to each other. Because of the gradual loss of concrete bonding at the surface of the plugin bars and tension strands during repeat cycles, the moment strength of the assembled connection was loading-history dependent. Obvious cyclic softening behaviors were presented such that the moment strength of QS3 and QS4 degraded rapidly under the loading phase with repeated cycles. However, the tested connections still presented reasonable load-bearing performance and a certain postyield strengthening ability, with the moment

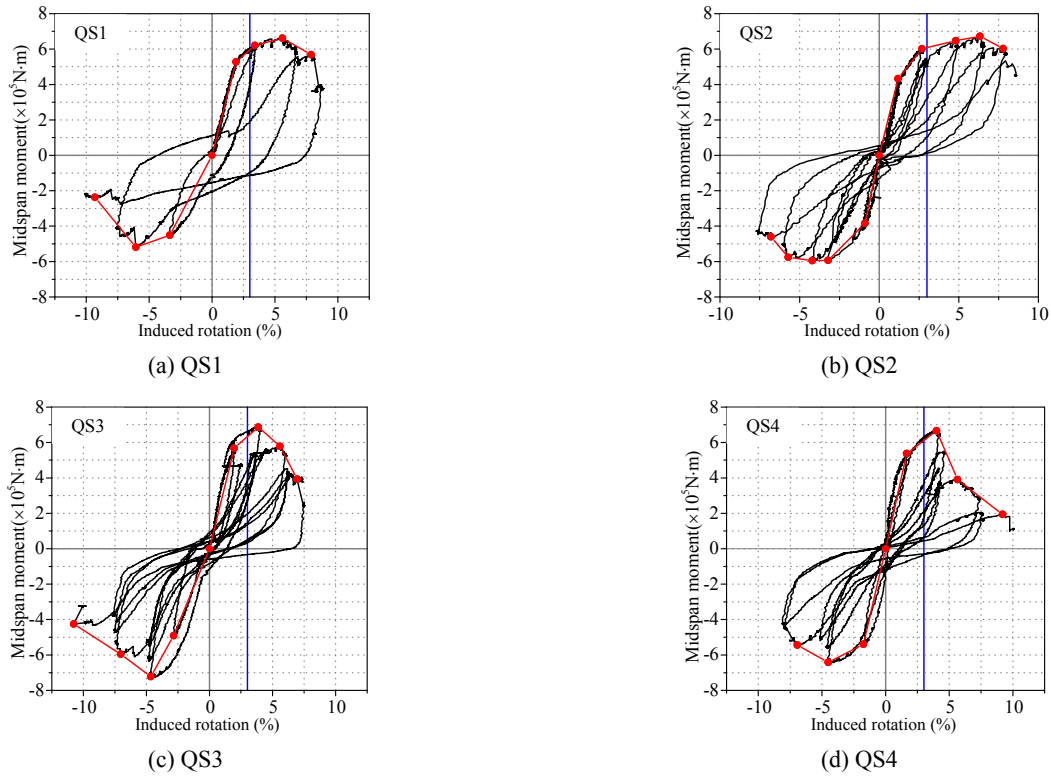


Fig. 16 Midspan moment-rotation relationships

strength remaining as the increasing trend before 3% rad (blue line in Fig. 16 gives the 3% rad rotation limit).

Fig. 17 shows the envelope curves for the four cyclic tests, which were obtained by connecting the maximum strength point at each load level from the hysteresis loops. With the same section dimension and similar plugin bar or strand settings, the four specimens displayed similar initial stiffnesses. A comparison of QS1 and QS2 indicated that the column length had little effect on the moment-bearing performance. QS1 and QS4 showed similar initial strength growth during the first two loading steps (after which QS4 underwent repeated cycles at $2\Delta y$), indicating that the shear studs had little effect on hysteresis performance. QS3 (with regional stretching) displayed a slight increase in the moment-bearing strength and a milder strength degradation than QS4 (with integral stretching). However, QS3 and QS4 still presented similar strength variation performances, and the effect of the stretching method was still not apparent.

In seismic design, a key index of the seismic connection performance is the energy dissipation capacity, which reflects the ability of a connection to absorb energy and reduce the seismic effects. An equivalent damping coefficient η is often used to quantify and compare the energy dissipation ability. The damping coefficient is calculated as the ratio of practical dissipated energy to the elastic potential energy at the maximum load amplitude. A larger η value indicates better energy dissipation capacity. A detailed calculation method for this coefficient can be found in reference (Yu *et al.* 2017). Because the maximum value is equal to $2/\pi$ when the enclosed region of the hysteresis loop is rectangular, another index (the energy efficiency factor η) was introduced according to Brando's

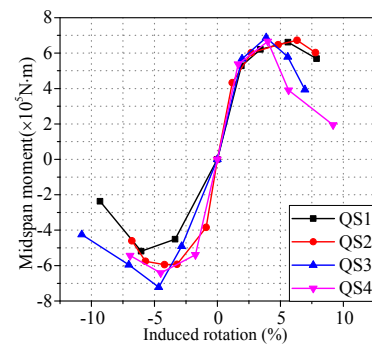


Fig. 17 Envelope curves

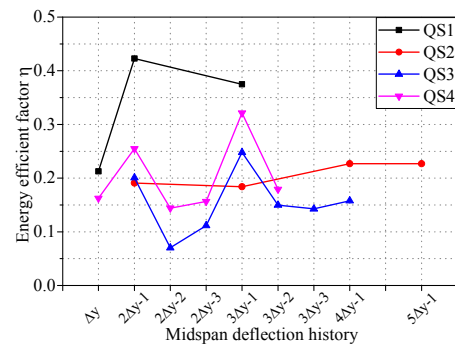


Fig. 18 Energy dissipation index

work (2013) as $\pi\eta/2$. In this case, the maximum value of η is 1.0, and the extent of energy dissipation can be easily evaluated. Fig. 18 compares the energy efficiency factors of

the four cyclic tests. During the test of QS1, dramatic concrete bonding failure and slipping behaviors continuously occurred. QS1 displayed a relatively wider hysteresis loop and nonlinear behaviors, resulting in the unusually higher η index than the others. While from QS2 to QS4, selected varying patterns can still be obtained. The following characteristics can be observed. The value of η increased with increasing deflection level but decreased during the repeated cycles. The short column connection (QS2) had a smaller energy dissipation than the others because of fewer plugin bars and strands for connection and the smaller moment arm design. The regional stretching case (QS3) had a slightly weaker η than the integral stretching case (QS4). The reason for this difference might be attributed to the comparatively smaller slippage allowance in the regional-stretched case due to clamping of the intermediate connector.

5.2 Simplified analysis and design method

The proposed pretensioned inter-module connection had assembled components, and the different construction induced different connecting abilities than those of the conventional steel frame connections. Referring to the joint classification method for a steel-framed connection, the proposed pretensioned connection presented semirigid behavior, but the bending stiffness and moment strength were all similar to the bounding limit of the pinned connection. Because the joint classification method in EC3 was mainly designed for the beam column connection in a frame structure, the applicability of the pinned joint simplification might not be accurate for inter-module connections. Then sometimes the moment-transferring ability at the inter-module connections need to be considered in the structural design. The monotonic and cyclic test results indicated that the moment-bearing strength was closely related to the tensioning or slipping states of the plugin bars and strands. Therefore, based on the strength development patterns and the failure modes observed in the tests, simplified strength calculations were proposed for this assembled connection. Because the connection displayed a moment-bearing ability similar to

that of the self-centering connections, a similar analysis method was adopted, which decomposed the resisted moment into two components

$$M_{total} = M_{bar} + M_{strand} \quad (1)$$

where M_{total} , M_{bar} , M_{strand} represent the total mid-span moment, the moment supplied by the plugin bars, and the moment supported by the strands. The test results indicated that the assembled sections were separated during the lateral loading process. In this work, we assumed that the neutral axis was located at the centerline of the edge bars/strands at the compression side, as shown in Figs. 19 and 20. In the connection design, the bonding length of the plugin bars was settled to ensure full use of the tension strength of the plugin bars. The plugin bars reached their yielding states prior to the occurrence of slipping. After yielding, contact slippage might occur, and the moment rotation curves began to exhibit stiffness and strength degradation. These yielding and contact-slipping behaviors occurred first at the outer bars. Once all of the tensioned plugin bars reached the yielding and slipping state, M_{bar} stopped increasing. Therefore, two working states were involved for M_{bar} . One state is the yielding state that can be used in structural design. Under this state, steel material yielding and contact slipping are only initiated at the outer layer plugin bars. The other state is the ultimate state, which represents the moment capacity of the assembled connection. Under this state, the remaining bars located away from the neutral axis all reached their yielding or slipping state. The calculation schemes of the two working states are given in Fig. 19, and the resulting moments M_{bar} for the two working states can be calculated. The tension forces at the outmost plugin bars are represented as $F_{bar,i}$, where i represents the locations of the plugin bars. With the section construction and material properties in Section 3.2, the yield strength and ultimate strength of plugin bars for specimens S1, S2, and QS1-QS4 can be calculated with the following equations

$$M_{bar}(yield) = \sum (f_{bar} \times A_{bar} \times e_0) + \sum [f_{bar} \times (e_i/e_0) \times A_{bar} \times e_i] \quad i = 1, 2 \quad (2)$$

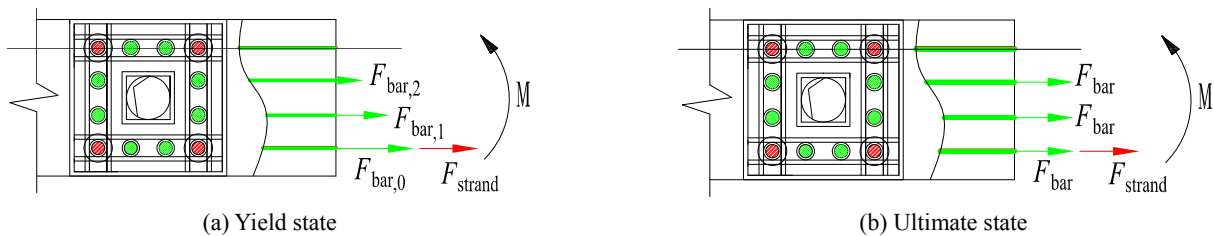


Fig. 19 Calculation diagram of wide-section connection (S1-S2, QS1-QS4)

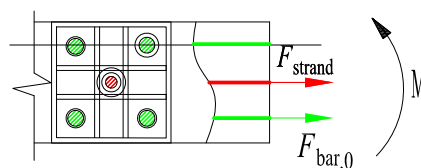


Fig. 20 Calculation diagram of small-section connections (S3-S6)

$$M_{bar}(ultimate) = \sum (f_{bar} \times A_{bar} \times e_i) \quad i = 0, 1, 2 \quad (3)$$

In this work, f_{bar} , A_{bar} , and e_i are the tension strength, section area, and offset distance of each HRB400 plugin bar from the rotation axis, respectively. For S3-S6 (Fig. 20), only two plugin bars were located away from the rotation axis. The yield and ultimate moment strength of the plugin bars are the same and could be calculated with Eq. (4).

$$M_{bar}(yield / ultimate) = \sum (f_{bar} \times A_{bar} \times e_0) \quad (4)$$

At the same time, the test data also indicated that the pretension force and contact bonding at the steel strands also contributed significantly to the moment-transferring performance of the assembled connection. Because of the high axial strength, the prestressed strands remained within the elastic state, even when the inside concrete yielded or the contact slipping states were widely spread. The test results also indicated that the tension strands were dislocated under severe concrete crushing and dramatic slipping at the concrete bonding surfaces. Moreover, if sufficient deflection was present, the strands eventually reached their yielding state or the ultimate strength state with wire breakage occurred. Therefore, we also define two working states for the pretension strands based on the contact bonding and slipping states of the steel strands. One state is the yielding state in which the surrounded concrete within the plugin bar anchorage length region (L_{ab}) reached the cracking limit. The other state is the ultimate state in which the tension strands reached their yield strength. The

yield moment and ultimate moment of the strands can be calculated from the following equations

$$M_{strand}(yield) = \sum (f_i \times \pi d \times L_{ab}) \times e_{strand} \quad (5)$$

$$M_{strand}(ultimate) = \sum (f_{strand} \times A_{strand} \times e_j) \quad (6)$$

Using the material strengths in Table 1 and Section 3.2, the moment strengths of the assembly connections can be calculated because the characteristic strengths are generally used in structural design. Two sets of moment-bearing strengths were calculated for the assembled connections: one used the measured material strengths to explore the effectiveness of the proposed simplified calculation method, and the other used the characteristic strengths to explore the reasonableness of the design values. The calculated strengths are given in Table 3, and comparisons with the test data are presented in Fig. 21.

The comparison indicated that for the strand and plugin bar arrangements in wide-section specimens (S1, S2 and QS1-QS4), the calculated strengths were similar to or slightly smaller than the corresponding test data, demonstrating the effectiveness and reasonableness of this evaluation method. For the small-section specimens, the calculated strengths were close to or slightly larger than the test data. Because of the single center strand construction of S3-S6, the assumed ultimate state of the tension strands might not be achievable, resulting in a predicted ultimate moment strength for S4 that is larger than the measured data. Case S3 or preliminary evaluation of the moment showed a strength development that is less than the

Table 3 Calculated moment strengths of tested assembly connections (N·m)

Connection type	With design material strength		With real material strength	
	Yield strength	Ultimate strength	Yield strength	Ultimate strength
S1	8.0×10^4	2.4×10^5	1.5×10^5	2.5×10^5
S2, QS1-QS4	2.9×10^5	5.1×10^5	3.9×10^5	5.6×10^5
S3, S4	9.6×10^4	1.3×10^5	1.2×10^5	1.4×10^5
S5, S6	8.7×10^4	8.7×10^4	9.9×10^4	9.9×10^4

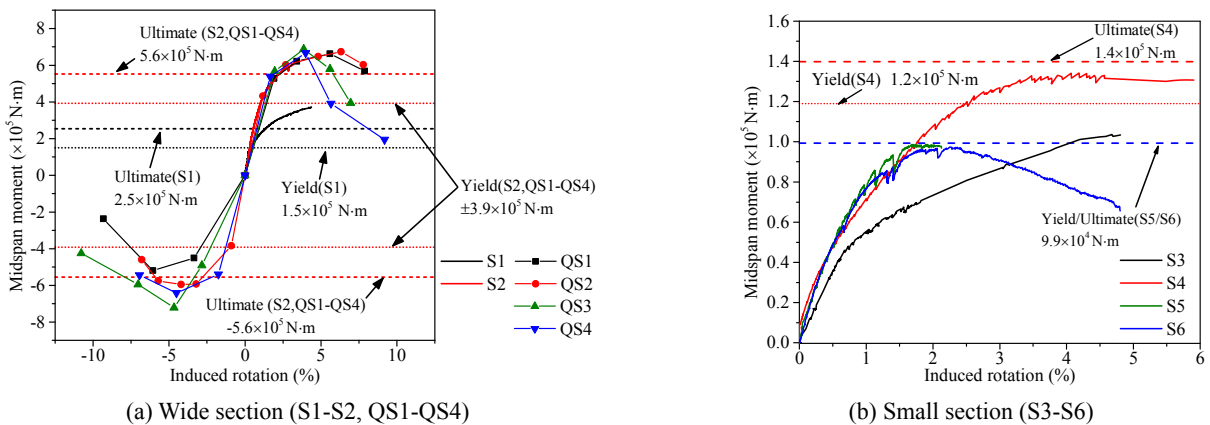


Fig. 21 Comparison of test results with calculated moment strength for real material data

analytical strength, which might have occurred because of the different stretching methods. The calculated moment resistance values with the material characteristic strengths were all smaller than the corresponding test data, especially for the yield strength calculations. From the perspective of structural design, the proposed calculation method can be used in precalculation transferring ability of the assembled inter-module connections. However, additional research is required in more detailed parametric studies and more precise analytical methods.

6. Conclusions

This paper proposed a pretension assembled inner-module connection design. The pretensioned connection used posttensioned strands to vertically connect the adjacent modular columns, ensuring a highly tightened connection for load transfer. The connection performance and moment-transferring mechanisms were studied using monotonic and cyclic lateral loading tests. Based on the test results, the following conclusions were obtained:

- In both the monotonic tests and cyclic loading tests, the proposed design displayed similar deflection and failure modes in which the assembled sections were separated from each other. The bending deformation of the specimens mainly originated from the separation gap at the assembled sections, with the modular columns remaining straight throughout the entire test. The connection displayed self-recovery behaviors in which the induced gap closed during unloading, and the lateral strength returned to its original value with little residual deflection remaining.
- The plugin bars and steel strands participated in load-bearing through bonding with the infill concrete during the early loading stage. With the increase of the bending extent, the concrete bonding to the plugin bars and steel strands was gradually lost, and only strand pretension remained for connection during the later loading periods.
- Referring to EC3, the assembled inter-module connection presented a semirigid connection, but the stiffness and strength levels were quite similar to those of the pinned connection boundary. For safety considerations, the proposed tensioned inter-module connection can be simplified as a pin connection during structural design.
- The moment-transferring performance of the connection was primarily related to the section construction and the arrangements of plugin bars and strands. The column length and shear studs presented limited effects. The in-depth influences and mechanisms still require further research.
- The connection moment strength can be calculated as the sum of the strand moment and plugin bar moment, and a simplified design method for strength evaluation was proposed. The effectiveness of the proposed calculation simplifications was validated. This method can be used in preliminary evaluation

of the moment-transferring ability of the proposed connection.

Acknowledgments

This research was sponsored by the National Key Research and Development Program of China (Grant NO. 2017YFC0703803), and the National Natural Science Foundation of China (Grant No. 51708402).

References

- Annan, C.D., Youssef, M.A. and El-Naggar, M.H. (2007), "Seismic performance of modular steel braced frames", *Proceedings of the Ninth Canadian Conference on Earthquake Engineering*, Ottawa, Ontario, Canada.
- Annan, C.D., Youssef, M.A. and El-Naggar, M.H. (2009), "Experimental evaluation of the seismic performance of modular steel-braced frames", *Eng. Struct.*, **31**(7), 1435-1446.
- Brando, G., Agostino, F.D. and Matteis, G.D. (2013), "Experimental tests of a new hysteretic damper made of buckling inhibited shear panels", *Mater. Struct.*, **46**(12), 2121-2133.
- Chen, Z., Li, H., Chen, A., Yu, Y. and Wang, H. (2017), "Research on pretensioned modular frame test and simulations", *Eng. Struct.*, **151**, 774-787.
- Chen, Y., Hou, C. and Peng, J. (2019), "Stability study on tenon-connected SHS and CFST columns in modular construction", *Steel Compos. Struct., Int. J.*, **30**(2), 185-199.
- Doh, J.H., Ho, N.M., Miller, D., Peters, T., Carlson, D. and Lai, P. (2016), "Steel Bracket Connection on Modular Buildings", *J. Steel Struct. Constr.*, **2**(2), 1000121.
- EN 1993-1-8 (2005), Eurocode 3: design of steel structures-part 1-8: design of joints, CEN, Brussels, Belgium.
- Farnsworth, D. (2014a), "Modular tall building design at Atlantic Yards B2", *Proceedings of CTBUH 2014 International Conference*, Shanghai, China.
- Fathieh, A. and Mercan, O. (2014), "Three-Dimensional, Nonlinear, Dynamic Analysis of Modular Steel Buildings", *Structures Congress 2014*, pp. 2466-2477.
- Fathieh, A. and Mercan, O. (2016), "Seismic evaluation of modular steel buildings", *Eng. Struct.* **122**, 83-92.
- GB 50010-2010 (2010), Code for Design of Concrete Structures; China Architecture and Building Press, Beijing, China.
- GB 50936-2014 (2014), Technical code for concrete filled steel tubular structures; China Architecture and Building Press, Beijing, China.
- Gunawardena, T., Ngo, T., Mendis, P. and Alfano, J. (2016a), "Innovative flexible structural system using prefabricated modules", *J. Architect. Eng.*, **22**(4), 05016003.
- Gunawardena, T., Ngo, T. and Mendis, P. (2016b), "Behaviour of Multi-Storey Prefabricated modular Buildings under seismic loads", *Earthq. Struct., Int. J.*, **11**(6), 1061-1076.
- JGJ101-96 (1996), Specification of Testing Methods for Earthquake Resistant Building; China Building Industry Press, Beijing, China.
- Lacey, A.W., Chen, W., Hao, H. and Bi, K. (2018), "Structural response of modular buildings – an overview", *J. Build. Eng.*, **16**, 45-56.
- Lawson, R.M., Ogden, R.G. and Bergin, R. (2012), "Application of Modular Construction in High-Rise Buildings", *J. Architect. Eng.* **18**(2), 148-154.
- Lawson, R.M., Ogden, R.G. and Goodier, C. (2014), *Design in Modular Construction*, CRC Press.

- Lee, S.S., Sang, S., Park, K.S., Hong, S.Y. and Bae, K.W. (2015), "Behavior of C-Shaped beam to square hollow section column connection in modular frame", *J. Kor. Soc. Steel Constr.*, **27**(5), 471-481.
- Liu, X.C., Xu, A.X., Zhang, A.L., Ni, Z., Wang, H.X. and Wu, L. (2015), "Static and seismic experiment for welded joints in modularized prefabricated steel structure", *J. Constr. Steel Res.*, **112**, 183-195.
- Lopezbarraza, A., Ruiz, S.E., Reyessalazar, A. and Bojorquez, E. (2016), "Demands and distribution of hysteretic energy in moment resistant self-centering steel frames", *Steel Compos. Struct., Int. J.*, **20**(5), 1155-1171.
- Rojas, P., Ricles, J.M. and Sause, R. (2005), "Seismic Performance of Post-tensioned Steel Moment Resisting Frames With Friction Devices", *J. Struct. Eng.-ASCE*, **131**(4), 529-540.
- Sharafi, P., Samali, B., Ronagh, H. and Ghodrati, M. (2017), "Automated spatial design of multi-story modular buildings using a unified matrix method", *Automat. Constr.*, **82**, 31-42.
- Srisangeerthan, S., Hashemi, M.J., Rajeev, P., Gad, E. and Fernando, S. (2018), "Numerical study on the effects of diaphragm stiffness and strength on the seismic response of multi-story modular buildings", *Eng. Struct.*, **163**, 25-37.
- Wang, Y., Ma, Q. and Yang, S. (2016), "Mechanical properties of beam-column connection joints using inner sleeve composite bolts in fabricated steel structure", *J. Tianjin Univ. (Science and Technology)*, **49**(Suppl.), 73-79.
- Yu, Y.J., Wang, X.X. and Chen, Z.H. (2017), "Evaluation on steel cyclic response to strength reducing heat treatment for seismic design application", *Constr. Build. Mater.*, **140**, 468-484.

BU

Appendix A

In the Chinese reinforced concrete design code (GB50010-2010, 2010), the anchorage length of the steel bar was calculated based on the designed strength of the steel bars. Given a piece of steel bar l_{ab} , the designed yield force of the steel bar is $f_d \pi d^2 / 4$ (where f_d is the designed yield strength for a HRB400 steel bar and $f_d = 360$ MPa; d is the diameter). Given the average contact bonding strength τ , the bonding force between concrete and steel bars is $\tau \pi d l_{ab}$. In the design code, the bonding strength τ was decided with concrete tension strength f_t and shape coefficient α of steel bars with the equation $\tau = f_t / 4\alpha$. In this work, α is 0.14 for a ribbed bar. Based on the equivalent relationship, the anchorage length was calculated as follows

$$\begin{aligned} l_{ab} &= \alpha f_d / f_t d \\ &= 0.14 \times 360 / 1.71 \times 32 = 943 \text{ mm} \end{aligned} \quad (7)$$

Appendix B

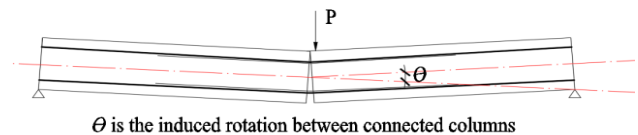


Fig. 22 Definition of bending rotation